3D numerical investigation of turbulent forced convection in wavy ducts with trapezoidal cross-section

Received April 1996
Revised November 1996

Masoud Rokni and Bengt Sundén
Division of Heat Transfer, Lund Institute of Technology, Lund, Sweden

Nomenclature

A_{cross}	=	cross-section area	T	=	temperature
A_w	=	area of the wall	T_h	=	bulk temperature
B	=	constant	T_p	=	point temperature
C_p	=	specific heat at constant pressure	T_w	=	wall temperature
C_E, C_D, C_t	=	closure coefficient	U^+	=	dimensionless velocity
$C_{\varepsilon 1}$,$C_{\varepsilon 2}$,$C\mu$	=	closure coefficient	U^*	=	friction velocity
D_h	=	hydraulic diameter	U_j	=	velocity
E	=	constant	U_m	=	mean velocity
f	=	fanning friction factor	$\overline{u_i u_j}$	=	turbulent shear stresses
$\overline{f_j t}$	=	buoyancy-driven heat flux	$\overline{u_j t}$	=	tubulent heat fluxes
h_{ov}	=	overall heat transfer coefficient	x_j	=	co-ordinate
k	=	kinetic energy	y^+	=	normal distance, see equation (29)
L	=	duct energy	β	=	cyclic pressure coefficient
$\dot{m}$	=	mass flow rate	δ_{ij}	=	Kroneckers delta
Nu	=	Nu-number	ε	=	dissipation
Nu_{ov}	=	overall Nu-number	ϕ	=	variable
Nu_x	=	average of Nu_{xp}	γ	=	cyclic parameter, see equation (54)
Nu_{xp}	=	local Nu-number at each point	Γ	=	diffusivity
P	=	pressure	η	=	distance normal to the wall
P^*	=	cyclic pressure	κ	=	Karman constant
P_k	=	production term	λ	=	cyclic parameter, see equation (21)
Pr	=	Prandtl number	μ	=	molecular viscosity
q	=	heat flux	μ_τ	=	turbulent viscosity
q_w	=	heat flux through the wall	θ	=	dimensionless temperature
Re	=	Reynolds number	ρ	=	density
S_{ij}	=	mean strain rate	σ	=	turbulent Prandtl number
$\mathring{S}_{ij}$	=	Oldroyd derivative of S_{ij}	Ω	=	cyclic temperature source term
S_ϕ	=	source term for variable ϕ	τ, τ_{ij}, τ_w	=	shear stresses

Introduction

Ducts with trapezoidal cross-sections occur frequently in industrial heat transfer equipment, e.g. cooling channels in gas turbines, compact heat exchangers, etc. Most such ducts are corrugated, curved or wavy in the main flow direction. Many investigations have shown that the heat transfer in

International Journal for Numerical Methods for Heat & Fluid Flow
Vol. 8 No. 1, 1998, pp. 118–141.

noncircular corrugated ducts is influenced by secondary motions in the plane perpendicular to the streamwise flow direction. The secondary motion, although small in magnitude, distorts the axial velocity profile and increases the friction factor.

The present investigation concerns numerical calculations of convective heat transfer and turbulent flow in wavy trapezoidal ducts and is a continuation of the investigation by Rokni and Sundén (1996) in straight ducts. The main purpose is to apply and evaluate a non-linear k-ε turbulence model (Speziale, 1987) for calculation of the turbulent stresses combined with the simple eddy diffusivity to calculate the turbulent heat fluxes. Also the generalized gradient diffusion hypothesis (GGDH) and the wealth equals earning times time (WET) (Launder, 1987) method for determination the turbulent heat fluxes are studied but to a less extent.

In the literature no numerical investigations have been presented on turbulent flow in corrugated or wavy trapezoidal ducts. Laminar numerical investigation has already been presented by Asako *et al.* (1993). Since the secondary motion and its velocity components are only a few percent of the main flow velocity, measurements of the secondary motion become very difficult. In this work, the focus is on fully developed periodic flow and further application of the computational method developed by the authors which has been applied successfully in straight ducts of various cross section (Rokni and Sundén, 1996). In particular the influence of the waviness on the thermal-hydraulic performance is of interest.

The modelling approach of this paper and the application to the wavy trapezoidal ducts is new and the investigation thus provides a contribution in the field of numerical methods for turbulent convective heat transfer in complex geometries.

Problem statement

In this study, corrugated ducts with different trapezoidal cross-sections are considered. A principle sketch of the duct and the geometrical parameters are shown in Figure 1.

This investigation concerns fully developed periodic turbulent flow and convective heat transfer in a three dimensional wavy duct. Periodic conditions are imposed at the inlet and outlet of the duct to achieve the fully developed state in an easy way. The wave length and amplitude of the duct are defined by relating them to the height of the duct.

The overall performance of the duct in terms of the friction factor and Nusselt number is to be determined numerically. The secondary flow motion as well as the temperature distribution in the cross-sectional plane are also of major concern.

Governing equations

The governing equations are the continuity, momentum and energy equations. Fully developed periodic turbulent flow and heat transfer is considered in this

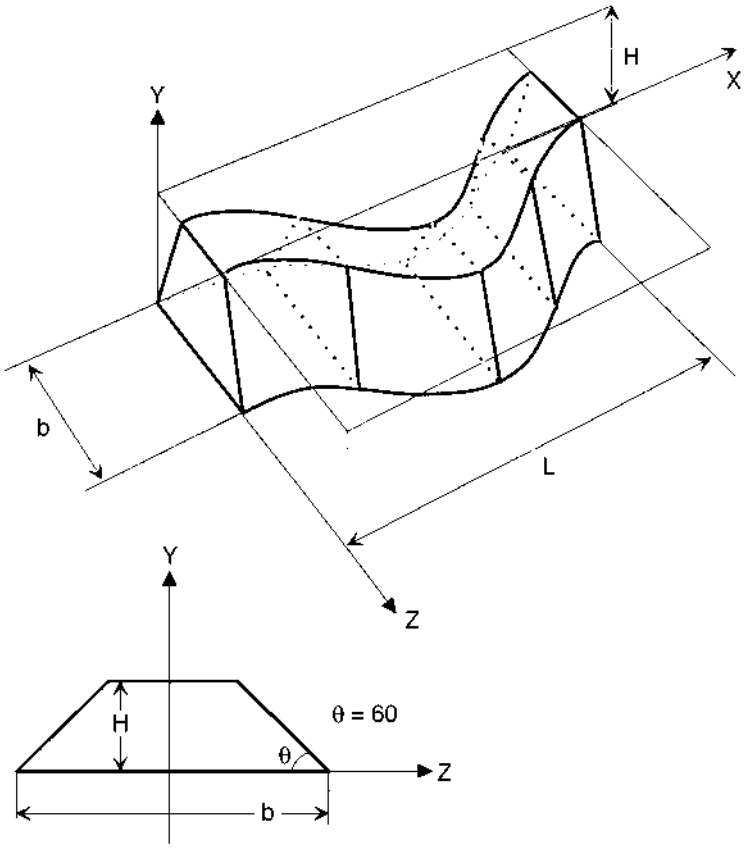

Figure 1.
Duct under consideration

investigation. The following assumptions are employed: steady state, no-slip at the walls, constant fluid properties and no natural convection. One then has:

$$\frac{\partial}{\partial x_j}\left(\rho U_j\right) = 0 \tag{1}$$

$$\frac{\partial}{\partial x_j}\left(\rho U_i U_j\right) = -\frac{\partial P}{\partial x_i} + \frac{\partial}{\partial x_j}\left[\mu\left(\frac{\partial U_i}{\partial x_j} + \frac{\partial U_j}{\partial x_i}\right)\right] + \frac{\partial}{\partial x_j}\left(-\rho\overline{u_i u_j}\right) \tag{2}$$

$$\frac{\partial}{\partial x_j}\left(\rho U_j T\right) = \frac{\partial}{\partial x_j}\left[\frac{\mu}{Pr}\frac{\partial T}{\partial x_j} + \left(-\rho\overline{u_j t}\right)\right] \tag{3}$$

The turbulent stresses ($-\rho\overline{u_i u_j}$) and turbulent heat fluxes ($-\rho\overline{u_j t}$) are modeled as described in the following sections.

Turbulence model for stresses

The most widely used two-equation turbulence model, the so called the k-ε model is also used here. It consists of two equations for the turbulent kinetic energy k and the dissipation rate of the turbulent kinetic energy ε. The conventional high Reynolds number k-ε model for steady state is given by

$$\frac{\partial}{\partial x_j}\left(\rho U_j k\right) = \frac{\partial}{\partial x_j}\left[\left(\mu + \frac{\mu_\tau}{\sigma_k}\right)\frac{\partial k}{\partial x_j}\right] + P_k - \rho\varepsilon \tag{4}$$

$$\frac{\partial}{\partial x_j}\left(\rho U_j \varepsilon\right) = \frac{\partial}{\partial x_j}\left[\left(\mu + \frac{\mu_\tau}{\sigma_\varepsilon}\right)\frac{\partial \varepsilon}{\partial x_j}\right] + C_{\varepsilon 1}\frac{\varepsilon}{k}P_k - C_{\varepsilon 2}\rho\frac{\varepsilon^2}{k} \tag{5}$$

where P_k is the production term expressed as

$$P_k = \tau_{ij}\frac{\partial U_i}{\partial x_j} = -\rho\overline{u_i u_j}\frac{\partial U_i}{\partial x_j} \tag{6}$$

Speziale (1987) proposed a non-linear constitutive relation for the k-ε model (for incompressible flow) which has the ability to predict secondary velocity motion (Rokni and Sunden, 1996; Speziale, 1987) perpendicular to the main flow direction in ducts. In this model, the description of the turbulent stresses is determined according to

$$\tau_{ij} = -\frac{2}{3}\rho k\delta_{ij} + 2\mu_\tau S_{ij} + 4C_D C_\mu \mu_\tau \frac{k}{\varepsilon}\left(S_{ik}S_{kj} - \frac{1}{3}S_{mn}S_{nm}\delta_{ij}\right) + 4C_E C_\mu \mu_\tau \frac{k}{\varepsilon}\left(\dot{S}_{ij} - \frac{1}{3}\dot{S}_{mm}\delta_{ij}\right) \tag{7}$$

where

$$S_{ij} = \frac{1}{2}\left(\frac{\partial U_i}{\partial x_j} + \frac{\partial U_j}{\partial x_i}\right) \tag{8}$$

and $\dot{S}_{ij}$ is the frame-indifferent Oldroyd derivative (Wilcox, 1993) of S_{ij} in the form of

$$\dot{S}_{ij} = \frac{\partial S_{ij}}{\partial t} + U_k\frac{\partial S_{ij}}{\partial x_k} - \frac{\partial U_i}{\partial x_k}S_{kj} - \frac{\partial U_j}{\partial x_k}S_{ki} \tag{9}$$

In equation (9), the first term on the right hand side is zero since we consider steady state condition. The turbulent eddy viscosity μ_τ is calculated by

$$\mu_\tau = \rho C_\mu \frac{k^2}{\varepsilon} \tag{10}$$

The standard values for the constants and closure coefficients in (4), (5), (7) and (10) have been used as shown below:

σ_k	σ_ε	$C_{\varepsilon 1}$	$C_{\varepsilon 2}$	C_D	C_E	C_μ
1.0	1.314	1.44	1.92	1.68	1.68	0.09

In the Speziale model, the non-linear terms (the terms in the brackets in equation (7)) are a form of quadratic terms which enables prediction of the secondary velocity field through channels.

Turbulence models for heat flux

The turbulent heat fluxes are expressed as:

(1) Simple eddy diffusivity (SED) based on the Boussinesq viscosity model as

$$\rho\overline{u_j t} = -\frac{\mu_\tau}{\sigma_T}\frac{\partial T}{\partial x_j} \tag{11}$$

where the turbulent Prandtl number σ_T is chosen to be 0.89. This model is the most common used model in the field of numerical calculation of the heat fluxes. It is also the basic model to determine the turbulent heat fluxes in this investigation.

(2) Generalized gradient diffusion hypothesis (GGDH) expressed by Daly and Harlow (1970) as:

$$\rho\overline{u_j t} = -\rho C_t \overline{u_j u_k}\frac{k}{\varepsilon}\frac{\partial T}{\partial x_k} \tag{12}$$

This model indicates, for example, that the streamwise heat flux in pipe flow can also be produced mostly by the radial temperature gradient by taking the non-isotropy into account (if $\partial T/\partial x$ is much smaller than $\partial T/\partial r$). A similar statement may be concluded in ducts of noncircular cross section.

(3) Wealth α earnings $\times$ time, named as the WET hypothesis (Launder, 1987a, 1987b) which actually is an economic statement. By applying it to the heat fluxes, this idea leads to: value of second moment α generation rate of second moment $\times$ turbulent time scale. One then has

$$\rho\overline{u_j t} = -\rho C_t \frac{k}{\varepsilon}\left(\overline{u_j u_k}\frac{\partial T}{\partial x_k} + \overline{u_k t}\frac{\partial U_j}{\partial x_k} + \overline{f_j t}\right) \tag{13}$$

where $\overline{f_j t}$ is the buoyancy-driven heat flux which is zero in the case of pure forced convection. Otherwise one can see that, in buoyancy-driven flow and in the absence of mean temperature or velocity gradients, a vertical heat flux can be driven by the temperature variance $\overline{t^2}$ ($f_j = -g_j t/T$ for perfect gas).

The constant C_t is set to 0.3 in both GGDH and WET models.

Periodic condition

Periodic means that the flow cross section varies in a cyclic manner along the main flow direction at sufficient large downstream distance. For a corrugated or wavy duct of periodically varying cross section, the velocity profile repeats itself successively in the fully developed region. This happens, of course, in a succession of cross sections that are separated from each other by the period length. Since this investigation concerns only the fully developed domain, there is no need to calculate the developing region. Applying a reasonable periodic condition to the velocity components enables a significant reduction of the computational times and cost, because the number of grid points in the main flow direction can be decreased considerably. The idea of using periodic conditions for calculation of fully developed region was initiated by Patankar *et al.* (1977) originally for corrugated surfaces. It has then been used by several authors, e.g. Prata and Sparrow (1984), Faghri and Asako (1984), Webb and Ramadhyani (1985), Rokni and Sundén (1996) etc.

It is obvious that the pressure P decreases in a duct since there must be a net mass flow in the positive x-direction. Therefore the pressure should be handled in a special way, it is instead expressed by

$$P(x,y,z) = -\beta x + P^*(x,y,z) \tag{14}$$

where βx is related to the global mass flow and β is a constant representing the non-periodic pressure gradient. P^* behaves in a periodic manner from cycle to cycle in the flow direction. Inserting equation (14) into the momentum equation (2) gives

$$\frac{\partial}{\partial x_j}\left(\rho U_i U_j\right) = \beta\frac{\partial x}{\partial x_i} - \frac{\partial P^*}{\partial x_i} + \frac{\partial}{\partial x_j}\left[\mu\left(\frac{\partial U_i}{\partial x_j} + \frac{\partial U_j}{\partial x_i}\right)\right] + \frac{\partial}{\partial x_j}\left(-\rho\overline{u_i u_j}\right) \tag{15}$$

where $\partial x/\partial x_i$ is equal to one in the x-direction (U-velocity) and zero in the y- and z-directions (V and W velocities).

It is also apparent that the temperature field does not repeat itself in the fully developed region while an appropriately defined dimensionsless temperature θ does. The dimensionsless temperature is defined in the periodic case as

$$\theta(x,y,z) = \frac{T(x,y,z) - T_w}{T_b(x) - T_w} \tag{16}$$

where T_b is the fluid bulk temperature and T_w is the constant wall temperature. Using this expression and inserting it into the energy equation (3) one obtains

$$\frac{\partial}{\partial x_j}\left(\rho U_j \theta\right) = \frac{\partial}{\partial x_j}\left[\frac{\mu}{Pr}\frac{\partial \theta}{\partial x_j}\right] + \Omega + \frac{\partial}{\partial x_j}\left(-\rho\overline{u_j\theta}\right) \tag{17}$$

where Ω is

$$\Omega = \lambda\left[\Gamma\frac{\partial\theta}{\partial x} + \frac{\partial}{\partial x}(\Gamma\theta) - \rho U\theta\right] + \Gamma\theta\left(\lambda^2 + \frac{\partial\lambda}{\partial x}\right) \tag{18}$$

and

$$\rho\overline{u_j\theta} = \frac{\rho\overline{u_j t}}{T_b - T_w} \tag{19}$$

In (18) λ is

$$\lambda = \frac{\partial(T_b - T_w)}{\partial x} / (T_b - T_w) \tag{20}$$

and $\Gamma = \mu/\mathrm{Pr}$. One can recognise that both λ and Ω are periodic parameters.

In the GGDH method , $\overline{u_j t}$ can be calculated from

$$\overline{u_j t} = -c_t\frac{k}{\varepsilon}(T_b - T_w)\left\{\overline{u_j u}\left(\lambda\theta + \frac{\partial\theta}{\partial x}\right) + \overline{u_j v}\frac{\partial\theta}{\partial y} + \overline{u_j w}\frac{\partial\theta}{\partial z}\right\} \tag{21}$$

In the WET method , it can be determined from

$$\overline{u_j t} = -c_t\frac{k}{\varepsilon}(T_b - T_w)\left\{\overline{u_j u}\left(\lambda\theta + \frac{\partial\theta}{\partial x}\right) + \overline{u_j v}\frac{\partial\theta}{\partial y} + \overline{u_j w}\frac{\partial\theta}{\partial z} + \overline{u_k t}\frac{\partial U_j}{\partial x_k}\right\} \tag{22}$$

Since the energy equation contains two unknowns, $\lambda(x)$ and $\theta(x, y, z)$, an additional condition is needed to close the problem. This condition may be obtained from the definition of the bulk temperature. In dimensionsless form one has

$$\int |U|\theta dA_{cross} = \int |U| dA_{cross} \tag{23}$$

where A_{cross} is the cross-sectional area perpendicular to the main flow direction. As mentioned previously, the shape of the non-dimensional temperature profile $\theta(x, y, z)$ repeats itself in its fully developed cyclic state.

Boundary conditions

Periodicity conditions are imposed at the inlet and outlet for all variables. It then follows

$$\Phi(x, y, z) = \Phi(x + L, y, z)$$

$$\Phi = U, V, W, \theta, P^*, k, \varepsilon, \overline{u_i u_j}, \overline{u_j\theta}, \lambda, S_{ij} \tag{24}$$

Momentum equations

The local Reynolds number near any wall becomes very small owing to the viscous influences. Therefore the turbulence models which are suggested for high Reynolds number become inadequate. To overcome this problem a special treatment should be considered for the grid points close to each wall. Generally, there are two methods to account for the wall effects in numerical calculations of turbulent duct flow. One is to employ a low-Reynolds number modelling, and the other is the wall function method. The latter is most economical and frequently applied in computational fluid flow and heat transfer. In this work the so-called universal log law or the law of the wall (Launder, 1987b) is considered. For the momentum equations one has

$$U^+ = \frac{U}{U^*} \cong \frac{1}{\kappa} \ln y^+ + B = \frac{1}{\kappa} \ln(Ey^+) \tag{25}$$

where

$$y^+ = \frac{\rho U^* \eta}{\mu} \tag{26}$$

In equation (25), $E = 9$ and the von Karman constant $\kappa = 0.41$.

The law of the wall is applied for both the velocity and temperature fields in the region near the walls. It is assumed that the region close to each wall consists of only two layers, "the viscous sublayer" and "the log layer". In the viscous sublayer the turbulent viscosity is much smaller than the molecular viscosity while in the log layer the turbulent viscosity is much greater than the molecular viscosity. The "buffer layer" is ignored. The point $y^+ = 11.63$ which usually is defined to dispose the intersection (transition) between these two layers is also used here. It is assumed that below this point the flow is purely viscous (i.e. the turbulent stress is negligible), and above this point the flow is assumed to be purely turbulent. Boundary conditions for the turbulent kinetic energy and dissipation rate of it are also applied. More details of the practical application are discussed in Rokni and Sundén (1996).

Temperature equation

A similar treatment is applied for calculating the temperature at the grid point adjacent to the wall. The heat flux across the viscous sublayer is assumed to be constant. The point $y^+ = 11.63$ is also defined here to dispose the intersection between the viscous sublayer and the log layer. In summary, the energy transport of heat is calculated from:

(1) In the turbulent region, by

$$\frac{q_w}{C_p} = \frac{\rho U^* (T_w - T_p)}{\sigma_T \left[U^+ + P\left(\frac{Pr}{\sigma_T}\right) \right]} \tag{27}$$

where the P-function is correlated from pipe flow data by Jayatillika (1966) as

$$P\left(\frac{Pr}{\sigma_T}\right) = 9.24\left[\left(\frac{Pr}{\sigma_T}\right)^{0.75} - 1\right]\left[1 + 0.28e^{\left(-0.007/\left(\frac{Pr}{\sigma_T}\right)\right)}\right] \quad (28)$$

(2) In the viscous sublayer, it is calculated by using the following relation:

$$\frac{q_w}{C_p} = \frac{\mu}{\eta Pr}(T_w - T_p) \quad (29)$$

The reader is referred to Rokni and Sundén (1996) for more details.

Specific considerations

A non-uniform grid distribution is employed in the plane perpendicular to the main flow direction. Close to each wall the number of grid points or control volumes is increased to enhance the resolution and accuracy.

A sophisticated computational method for generation of control volumes was developed to generate the grid points in the cross sectional area with different stretching of the grid points close to each wall in a simple manner. This method allows one to choose as close to each wall as one wishes, the beginning of the clustering of the grid points and how. It also allows one to vary the distance between the points adjacent to the walls individually for each wall. This method is rather complicated and is beyond the discussion of this paper. The procedure is available from the authors on request. Figure 2 shows a typical distribution of grid points.

Additional equations

The normal velocity at any point can be determined as

$$\overline{U} = \frac{U_k n_k}{(|n_i|)^2} n_i \quad (30)$$

and its absolute mean value can be calculated by

$$U_m = \frac{|U_i n_i|}{\sqrt{(|n_k|)^2}} \quad (31)$$

The mass flow can then be derived by integrating equation (31) over cross section area. The Re-number is determined by using the hydraulic diameter.

The Fanning friction factor is defined by

$$f = \frac{\beta D_h / 4}{\rho U_m^2 / 2} \quad (32)$$

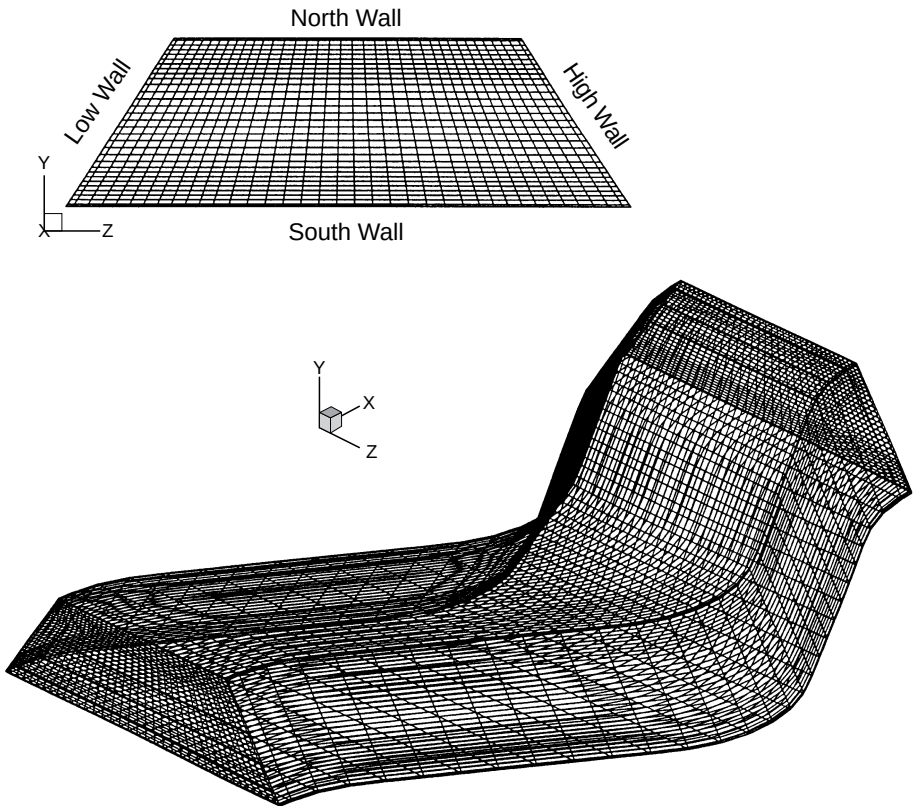

Figure 2.
Distribution of grid points

The calculated friction factor is compared with the Prandtl friction law (Ösizik, 1977). From a heat balance over the duct, one can determine the overall heat transfer coefficient for the duct. One then finds

$$\mathrm{Nu}_{ov} = \frac{2A_{cross}}{A_w}\frac{(1-\gamma)}{(1+\gamma)}\mathrm{Pr}\,\mathrm{Re} \tag{33}$$

where γ in the cyclic case can be derived as

$$\gamma = \exp\left(\int_0^L \lambda dx\right) \tag{34}$$

(and λ is defined in equation (20)).

This Nu-number is compared to that of the Dittus-Boelter equation (Ösizik, 1977) for circular ducts by using the hydraulic diameter.

To determine the local heat transfer at the point adjacent to the wall for each cross sectional area one may calculate the local Nu-number to the corresponding point as follows

(a) If $y^+ \leq 11.63$ at the wall adjacent grid point (index p) Nu_{xp} is found as

$$Nu_{xp} = D_h \frac{\theta_p}{\eta} \tag{35}$$

where θ_p is the dimensionsless temperature at the point adjacent to the wall.

(b) For $y^+ \geq 11.63$, the Nu_{xp} is found from

$$Nu_{xp} = \frac{Pr\, D_h}{\mu} \frac{\rho U^* \theta_p}{\sigma_T \left[U^+ + P\left(\frac{Pr}{\sigma_T} \right) \right]} \tag{36}$$

where the P-function is given in equation (28). The details are discussed in Rokni and Sundén (1996). The Nu_{ov} number shows the overall Nusselt number in the duct while Nu_{xp} shows the local Nusselt number in points adjacent to the wall.

Numerical solution procedure

In order to extend the capabilities of the general finite-volume technique and to deal with complex geometries and complex flows, a curvilinear co-ordinate transformation with boundary fitted co-ordinate method is applied. This method allows one to map the complex flow domain in the physical space to a rectangular domain in the computational space. This means that the Cartesian co-ordinate system x_i is replaced by a general non-orthogonal co-ordinate system ξ_i.

The momentum equations are computationally solved for the velocity components on a non-staggered grid arrangement. All the calculated variables are thus stored in the centre of the control volume. The Rhie-Chow interpolation method is used to interpolate the velocity components to the control volume faces from the grid points. The SIMPLEC-algorithm (Raithby and Schneider, 1988) is employed to handle the pressure velocity coupling. SIP (Stone, 1968) and TDMA (Patankar, 1980) based algorithms are used for solving the equations. The convective terms are treated by the hybrid scheme (Patankar, 1980) while the diffusive terms are treated by the central-difference scheme. It should be noted that only the hybrid scheme could be used for solving the equations in order to reach the convergence criterion 10^{-4}. Other higher order schemes such as van Leer (1974) (bounded) and QUICK (Leonard, 1979) (unbounded) were found to be more or less unstable in reaching this criterion.

The numerical procedure is based on solving the general equation

$$\frac{\partial}{\partial t}(\rho\Phi) + \frac{\partial}{\partial x_j}(\rho\Phi U_j) = \frac{\partial}{\partial x_j}\left[\Gamma_\Phi \frac{\partial \Phi}{\partial x_j}\right] + S_\Phi \qquad (37)$$

Accuracy and reliability of the numerical method

This investigation is an extension of the work by Rokni and Sundén in the field of development, application and calculation of turbulent heat and fluid flow in complex geometries. Therefore the reader is referred to the previous work of the authors (Rokni and Sundén, 1996). They have successfully implemented all the mentioned turbulence models and calculation methods (in previous sections) in a three dimensional non-orthogonal computational program. They also applied their numerical method for prediction of turbulent secondary velocity vectors and convective turbulent heat transfer in straight ducts with different cross section. They showed, for example, that the Nu-number in a straight square channel follows the Dittus-Boetler equation very well; a result which has been shown experimentally. They also predicted eight secondary motions at the cross section of a straight square duct, which is also shown by experiment. They could successfully prove the reliability of their computational method in complex geometries. Influences of grid size, computational parameters, etc. were revealed and the details can be found in Rokni and Sundén (1996). A discussion of the accuracy in the program and the successful implementation of the presented models and formulas can be found in that reference.

Sample calculations

The Prandtl number was set to 0.72 and the Reynolds number was varied from 7,000 to 72,000 by choosing appropriate values of β, the per-cycle pressure gradient. The computations were terminated when the sum of absolute residuals normalized by the inflow was below 10^{-4} for all variables. To achieve this convergence criterion, the under-relaxation factor was set to 0.04 to 0.08 for different variables and depending on the case and the Re-number. The calculations were carried out on DEC 3000/400 and ALPHA STATION 200 $^{4/233}$ AXP computers. Based on the previous investigation (Rokni and Sundén, 1996) and to have reasonable computational times and costs, 32 times 38 grid points were chosen in the y- and z-directions while 30 grid points were chosen in the x-direction. The overall friction factors and Nu-numbers, which are most interesting from an engineering point of view, do not change significantly if the number of grid points is further increased in the cross section area. However, local values of the turbulent stresses are somewhat dependent on the number and distribution of the grid points.

The corrugation of the ducts is described by the following relations: ($'A_x(x)'$ stands for the amplitude of corrugation or wave, A is the maximum amplitude and H is the duct height. The relations given are convenient to use in the

computer code and are based on expected geometries in eventual industrial applications of this duct type.

a) L=7.5H and A =1H

$$
\begin{aligned}
0 < x < 0.4021H &\Rightarrow A_x(x) = 1.35H - \left\{(1.35H)^2 - x^2\right\}^{0.5} \\
0.4021H < x < 3.3479H &\Rightarrow A_x(x) = 0.0613H + 0.2979(x - 0.4021H) \\
3.3479H < x < 4.1521H &\Rightarrow A_x(x) = -0.35H + \left\{(1.35H)^2 - (x - 3.75H)^2\right\}^{0.5} \\
4.1521H < x < 7.0979H &\Rightarrow A_x(x) = 0.0613H - 0.2979(x - 7.0979H) \\
7.0979H < x < 7.5H &\Rightarrow A_x(x) = 1.35H - \left\{(1.35H)^2 - (x - 7.5H)^2\right\}^{0.5}
\end{aligned} \tag{38}
$$

b) L=7.5H and A =2H

$$
\begin{aligned}
0 < x < 0.7645H &\Rightarrow A_x(x) = 1.35H - \left\{(1.35H)^2 - x^2\right\}^{0.5} \\
0.7645H < x < 2.9855H &\Rightarrow A_x(x) = 0.2375H + 0.6866(x - 0.7645H) \\
2.9855H < x < 4.5145H &\Rightarrow A_x(x) = 0.65H + \left\{(1.35H)^2 - (x - 3.75H)^2\right\}^{0.5} \\
4.5145H < x < 6.7355H &\Rightarrow A_x(x) = 0.2375H - 0.6866(x - 6.7355H) \\
6.7355H < x < 7.5H &\Rightarrow A_x(x) = 1.35H - \left\{(1.35H)^2 - (x - 7.5H)^2\right\}^{0.5}
\end{aligned} \tag{39}
$$

c) L=15H and A =2H

$$
\begin{aligned}
0 < x < 0.3787H &\Rightarrow A_x(x) = 1.35H - \left\{(1.35H)^2 - x^2\right\}^{0.5} \\
0.3787H < x < 7.1213H &\Rightarrow A_x(x) = 0.0542H + 0.2805(x - 0.3787H) \\
7.1213H < x < 7.8787H &\Rightarrow A_x(x) = 0.65H + \left\{(1.35H)^2 - (x - 7.5H)\right. \\
7.8787H < x < 14.621H &\Rightarrow A_x(x) = 0.0542H - 0.2805(x - 14.621H) \\
14.621H < x < 15H &\Rightarrow A_x(x) = 1.35H - \left\{(1.35H)^2 - (x - 15H)^2\right.
\end{aligned} \tag{40}
$$

By using these equations and the dimensions given in Table I, four ducts with different geometry are considered.

Table I. Ducts under consideration

Case	L	A	b/H	b	Base-angle
1	7.5 H	1 H	3	0.006	60°
2	7.5 H	2 H	3	0.006	60°
3	7.5 H	1 H	3	0.006	45°
4	15 H	2 H	3	0.006	60°

As is seen from Table I, the wave length and amplitude of all cases considered are related to the height of the duct. Case 1 is considered as reference case and calculations for other cases are compared to this case. One case is calculated for a large range of Re-numbers while for the other cases only a few Re-numbers are considered, since the influence of the geometry is of most interest.

Results and discussion

Secondary velocity fields at different planes

The predicted secondary motion by the Speziale's non-linear k-ε model, at different planes perpendicular to the U-velocity are shown in Figure 3. This means that the depicted secondary velocity plane is not always perpendicular to the main flow direction. This figure concerns case 1 at Re-number about 18,000. However, these secondary motions are predicted at all Re-numbers in all cases considered. These motions are of major concern since they redistribute the turbulent kinetic energy at the cross section of a duct, which in turn increases the accuracy of heat flux calculations and temperature field distributions. The figure at the top shows the secondary velocity vectors at the inlet of the duct and the figure at the bottom shows these flow motions at the middle of the considered duct. The secondary velocities are also shown at one-sixth and one-third of the periodic length of the duct. Figure 4 concerns the main flow field from a different point of view (XY- and XZ-planes). One can see that there exists a tendency of recirculation at the mentioned planes, while the ratio of the amplitude to the wavelength of the duct is relatively small. The recirculations are more obvious for the duct of case 2. These figures reveal the complexity of the turbulent flows in the considered ducts.

Temperature fields at different cross sections

The dimensionsless temperature fields for the duct considered (case 1) in Figure 3 are shown in Figure 5. One can see how the temperature gradient varies from one cross section of the duct to another. As expected, the temperature gradient near the high wall in the middle of the duct is larger than those at the inlet of it. Increasing the amplitude of a duct will increase these gradients and thus increase the heat transfer through the high and low walls.

Overall Nu-number

Figure 6 shows the calculated Nu-number for case 1 compared with Dittus-Boelter equation and Figure 7 presents the calculated Nu-number for all cases considered. One clearly observes from these figures that the Nu-number is strongly dependent on the Re-number.

A general conclusion can be drawn here for case 1 since the Re-number is varied between 7,000 to 72,000. It is evident from Figure 6 that the calculated Nu-number for a duct with the geometry of case 1 is much higher than that

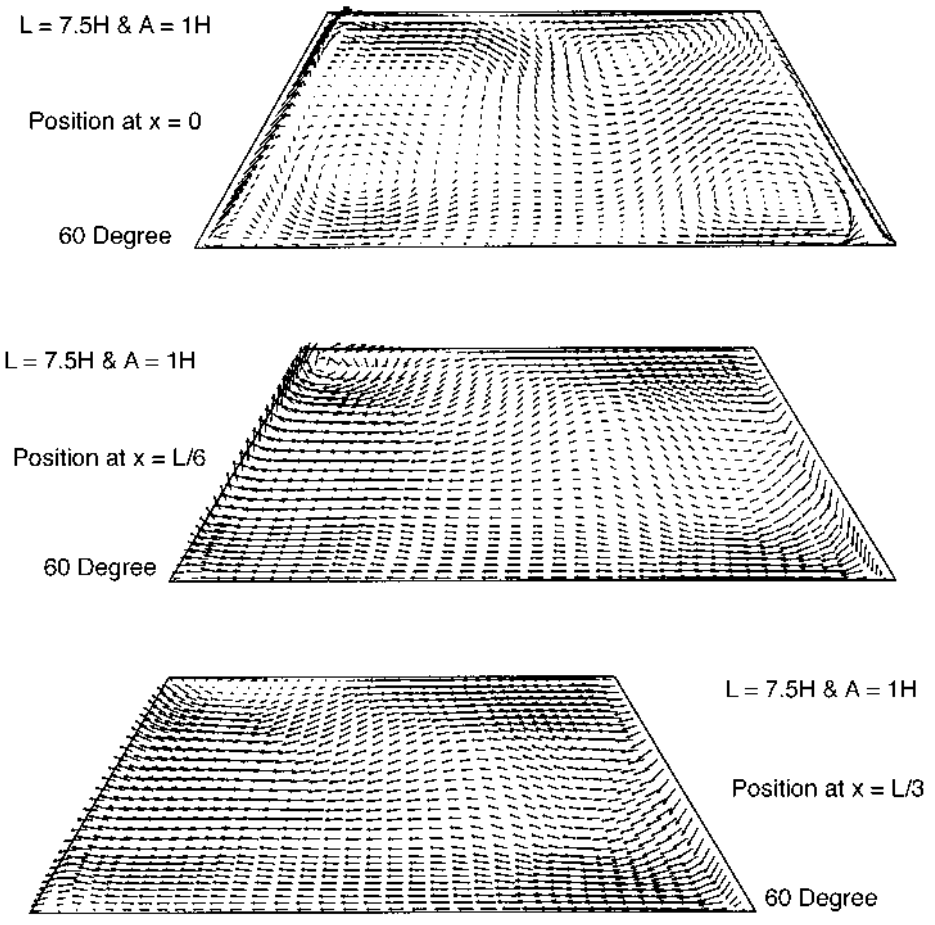

Figure 3.
The predicted secondary velocity motions for case 1 at different cross section areas. Re-number is about 18,000. From the top to the bottom, one finds changing of the secondary motions at the inlet of the channel to the middle of it

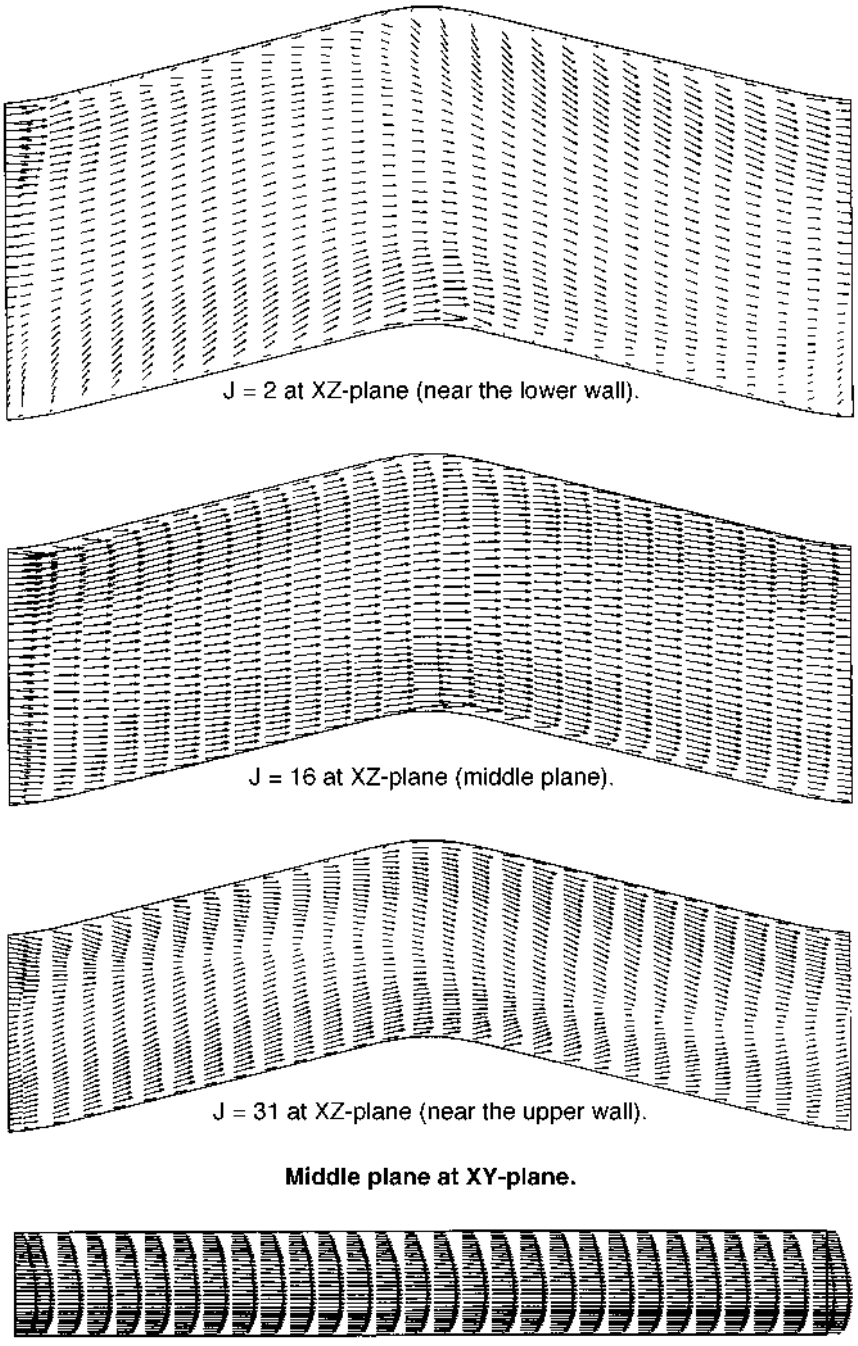

Figure 4.
Predicted main flow profiles from different points of view

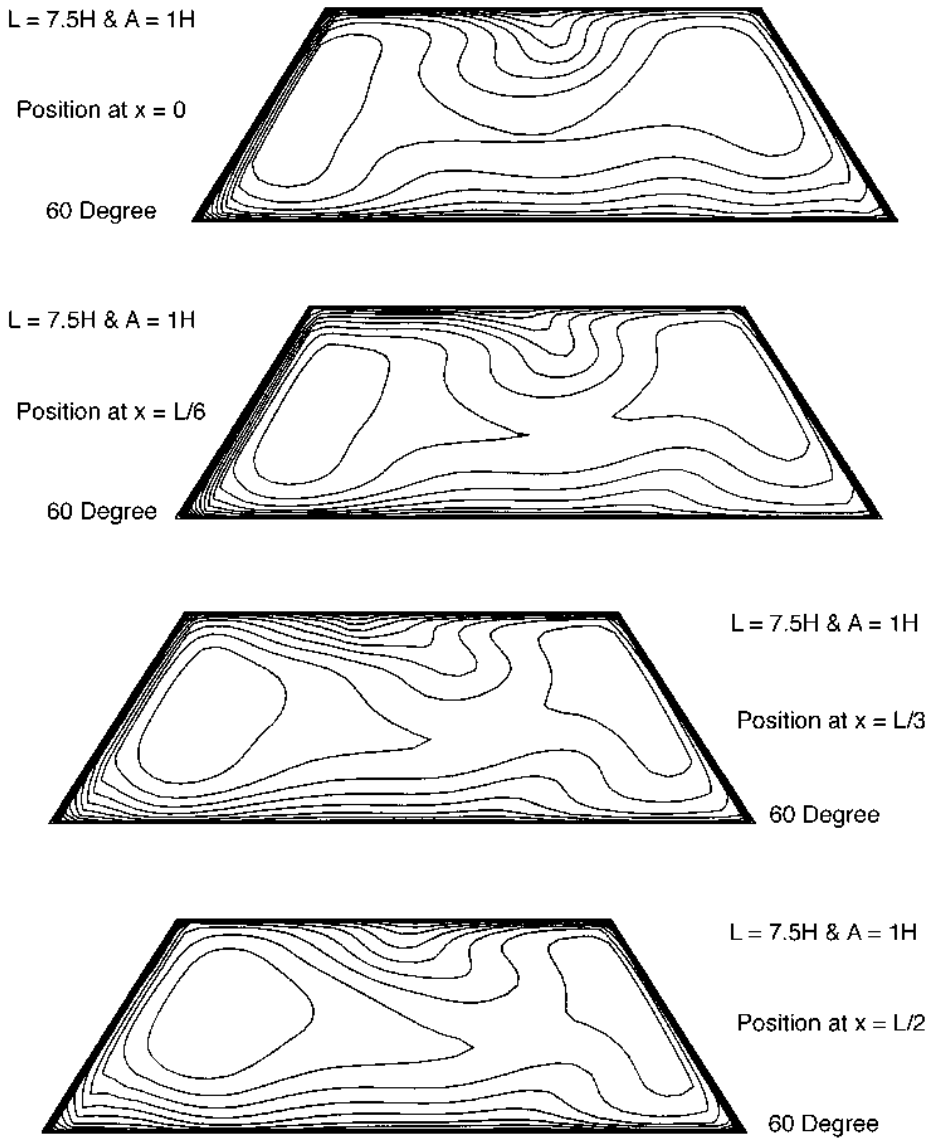

Figure 5.
The predicted temperature profile for case 1 at different cross section areas. Re-number is about 18,000. From the top to the bottom, one finds changing of the temperature distribution at the inlet of the channel to the middle of it

predicted by Dittus-Boelter equation which is valid for ducts with circular and square cross sections. However, the calculations show that the Nu-number for this kind of duct (case 1) can be estimated from the following equation within ±5 per cent.

$$Nu_{case\ \#1} = 0.03197\,\mathrm{Re}^{0.8}\,\mathrm{Pr}^{0.3} = 1.39x0.023\,\mathrm{Re}^{0.8}\,\mathrm{Pr}^{0.3} \quad (41)$$

In other words the Nu-number for this duct geometry (and for all the Re-numbers considered) is about 39 per cent higher than that for straight ducts

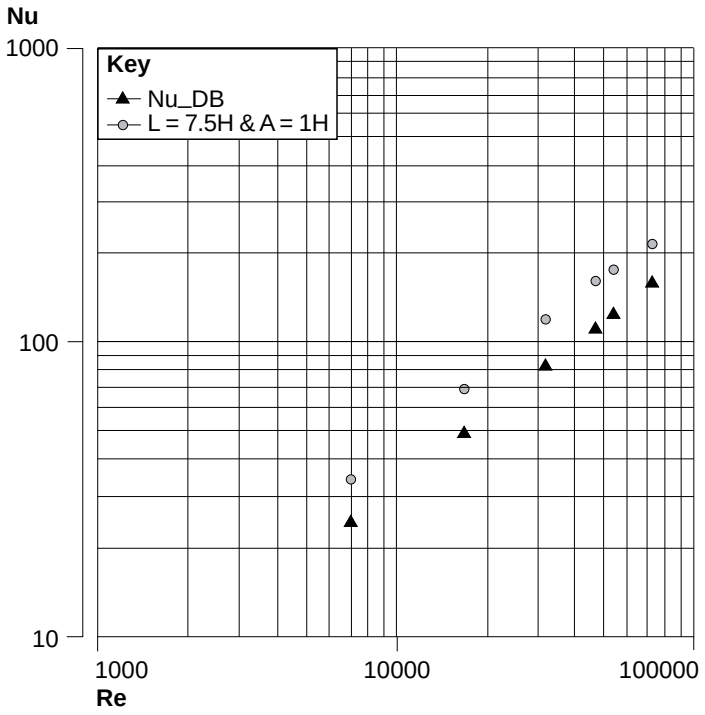

Figure 6.
Calculated overall Nu-number as function of Re-number for case 1 compared with Dittus-Boelter equation

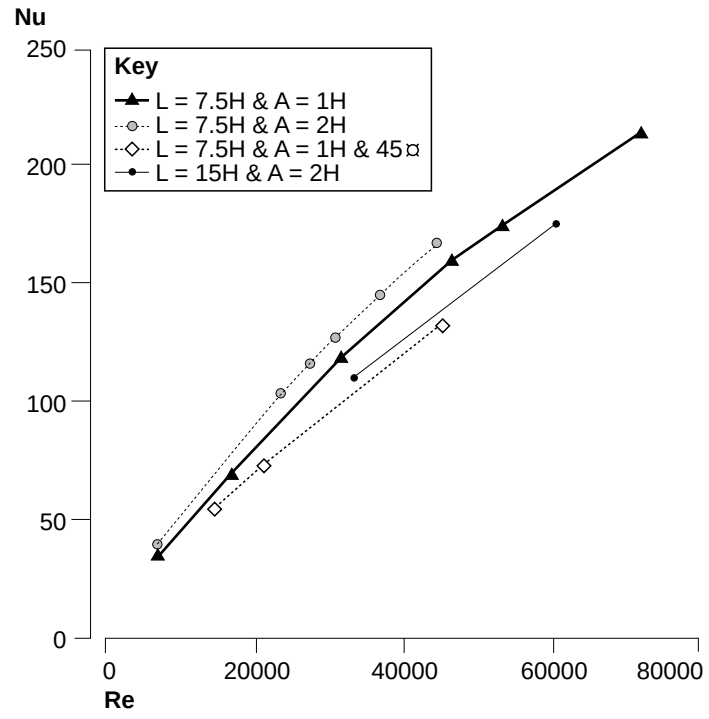

Figure 7.
Calculated Nu-number for all cases considered

In other words the Nu-number for this duct geometry (and for all the Re-numbers considered) is about 39 per cent higher than that for straight ducts with circular and square cross sections.

Preliminary studies indicate the following formulae for the Nusselt number of the other cases. However, it should be noted that only a limited number of Reynolds numbers were considered since the interest is mainly on the principal influence of the geometry.

$$Nu_{case\ \#2} = 0.03611\,\mathrm{Re}^{0.8}\,\mathrm{Pr}^{0.3} = 1.57x0.023\,\mathrm{Re}^{0.8}\,\mathrm{Pr}^{0.3} \tag{42}$$

$$Nu_{case\ \#3} = 0.0280\,\mathrm{Re}^{0.8}\,\mathrm{Pr}^{0.3} \tag{43}$$

$$Nu_{case\ \#4} = 0.0288\,\mathrm{Re}^{0.8}\,\mathrm{Pr}^{0.3} \tag{44}$$

It should be noted that the high reliability of the calculated overall Nu-number has already been proved in previous investigations by Rokni and Sundén.

By comparing the results, it is found that case 2 provides the highest Nusselt numbers. A reduction of the wave amplitude (case 1) reduces the Nusselt number by about 12 per cent while an increase in wavelength (case 4) reduces the Nusselt number by 20 per cent. By comparing case 1 and case 3 it is found that the base angle 60° is more efficient than 45°. However, all the considered cases enhance the heat transfer both in comparison with straight ducts governed by Dittus-Boelter's equation and straight trapezoidal ducts (in their fully developed conditions). In Rokni and Sundén (1996) it has been found that the predicted Nu-number by SED for a straight trapezoidal duct is close to those of the Dittus-Boelter's equation.

Local Nu-number

It might be interesting to know how the local Nu-number changes as the flow moves into the duct. The local Nu-number is strongly dependent on the y^+ values at the points adjacent to the wall. It is well known that the law of the wall is best valid for $y^+ > 30$. In a corrugated duct it is very difficult to adjust the distance between the grid points closest to the wall and the wall, in order to get more appropriate values for y^+. In all calculations in this investigation it was attempted to have an average y^+ value greater than 40 at the wall proximity. But there exist some points which have y^+ values less than 30. In order to decrease the uncertainty about the local Nu-number, one may normalize these values by the maximum local Nu-number for each cross section area. This is adopted in Figure 8. One may imagine how the local Nu-number varies from the north-wall to the high-wall and then to the south-wall and low-wall. The main flow direction is from west to east. The figure shows clearly that the predicted Nu-number at the inlet of the module of the channel

is lower than that inside the duct. This is explained by the flow field occurring at the various positions along the module length. At any place where two secondary motions meet each other and change direction, this results in a sudden drop and rise in the Nu-number. This is, of course, more obvious at the corners.

Friction factor

The predicted Fanning friction factors for the duct of case 1 are compared with those for a straight duct with identical cross section in Figure 9. This figure reveals that even a slight corrugation of a duct will considerably increase its friction factor.

Straight ducts with trapezoidal cross section were considered by Rokni and Sundén (1996). Their results can be used to normalize the calculated friction factors. The results are shown in Figure 10 where f0 corresponds to the friction factor of a corresponding straight duct. From the figure it is evident that an increase in the amplitude of the waviness results in a very high friction factor. The wavelength is also important.

Figure 10 shows also that the friction factor depends more on the corrugation of the duct than the shape of the cross section area.

From Figure 10 and equation (42) it is obvious that to achieve an enhancement of the heat transfer coefficient by 60 per cent one has to increase the pressure drop by a factor of more than six. This means that the pressure drop penalty is quite high and the kind of corrugation investigated is not the most efficient one. However, it should also be possible to find the most efficient combination of the geometry parameters in this case but that is beyond the scope of the present investigation.

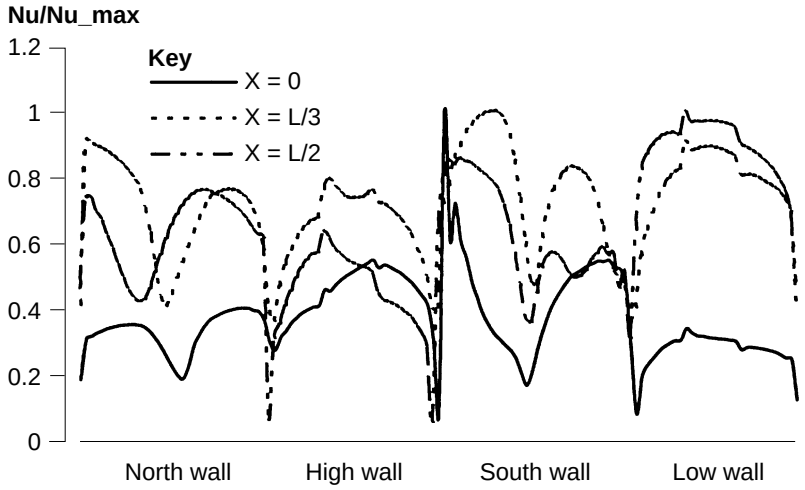

Figure 8.
The local Nu-number at different cross sections for case 1 with Re-number about 17,000. From left to the right, the predicted local Nu-number at the north-wall to the high-wall, south-wall and to the low-wall. See also Figure 2

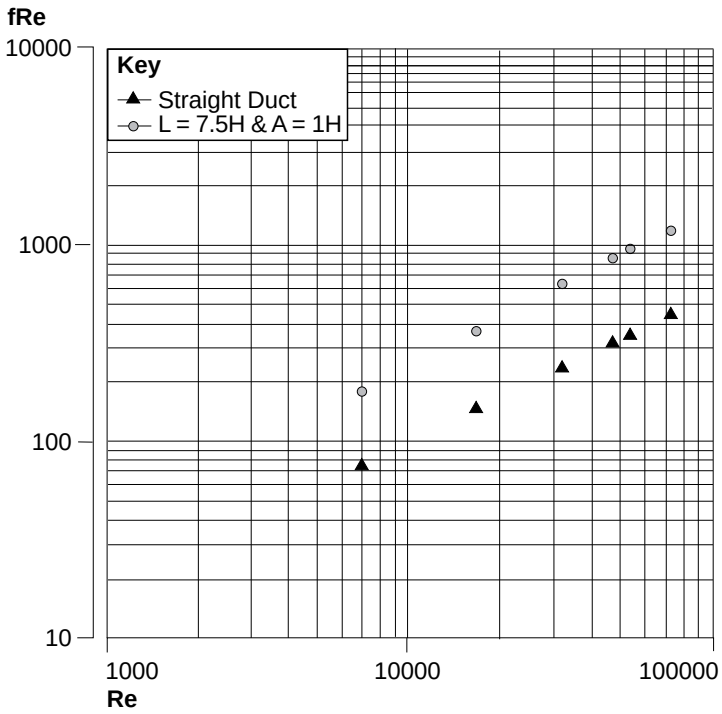

Figure 9.
Calculated fanning friction factor as function of Re-number for case 1 in comparison with corresponding straight duct

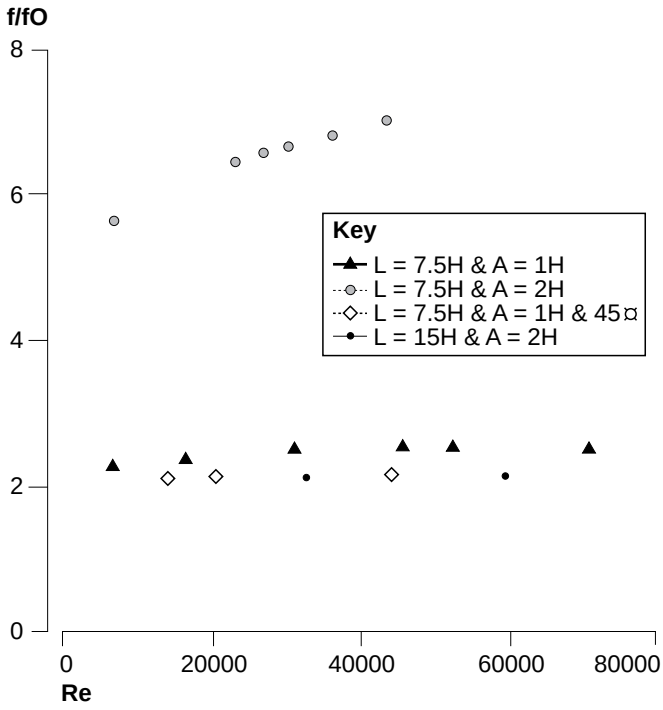

Figure 10.
Calculated friction factor normalized by the straight trapezoidal duct (f0)

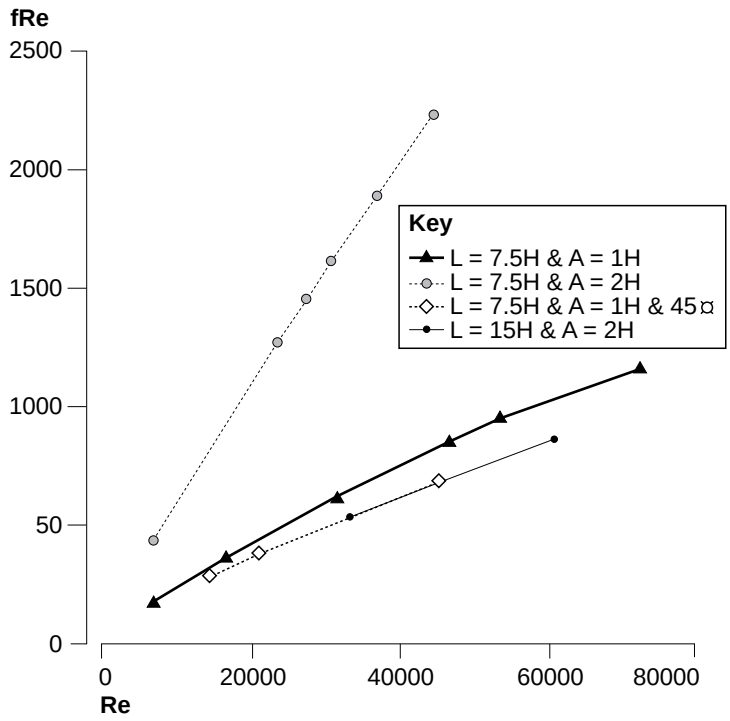

Figure 11. Calculated fRe-number for the considered ducts as function of Re-number

In order to distinguish the friction factor for different cases and different Re-numbers, the Fanning friction factor times Re-number is plotted as function of Re-number in Figure 11. Even in this figure, one can see that the friction factor is strongly dependent on the Re-number.

Comparison between GGDH, WET and SED

To calculate the turbulent heat fluxes by the GGDH and WET methods and reach the convergence criterion 10^{-4} was indeed very difficult for the present application. Therefore, only one case with one Re-number was considered to show how these models affect the Nu-number. The results are shown in Table II.

Thus it is found that the improved models do not change the results significantly.

Model	Re-number	Overall Nu-number
SED	24942.2	91.1
GGDH	24942.2	91.4
WET	24942.2	92.1

Table II. Calculated overall Nu-number with different models for turbulent heat fluxes

Conclusions

A numerical investigation for prediction of turbulent forced convection in wavy channels has been presented. Speziale's non-linear k-ε model is used to predict the secondary velocity fields and the simple eddy diffusivity concept is used to calculate the turbulent heat fluxes. The results are presented in terms of Nu-numbers and friction factors.

Different formulas are suggested for estimation of Nu-number in different ducts. It is shown that increasing the waviness of a duct increases the Nu-number and friction factor. Nu-number depends on the amplitude, wave length and exact cross section area of a channel. However, the friction factor depends mostly on the amplitude of the duct.

It has been found that the enhancement of heat transfer is accompanied by a very high pressure drop penalty.

References

Asako, Y., Faghri, M. and Sundén, B. (1996), "Three dimensional laminar forced convection in wavy channel with trapezoidal cross section", in Celata, G.P., Di Marco, P. and Mariani, A. (Eds), *2nd European Thermal-Science and 14th UIT National Heat Transfer Conference*, pp. 1097-104, Edizioni ETS.

Daly, B.J. and Harlow, F.H. (1970), "Transport equations in turbulence", *Physics of Fluids*, Vol. 13, pp. 2634-49.

Faghri, M. and Asako, Y. (1984), "Numerical determination of heat transfer and pressure drop characteristics for converging-diverging flow channel", *ASME Winter Annual Meeting*, Paper No. 84-WA-HT-12.

Jayatillika, C.L.V. (1966), "The influence of Prandtl number and surface roughness on the laminar sublayer to momentum and heat transfer", Imperial College, Mech. Eng. Dept., Report TWF/R/2.

Launder, B.E. (1987a), "On the computation of convective heat transfer in complex turbulent flows", *J. Heat Transfer*, Vol. 110, pp. 1112-28.

Launder, B.E. (1987b), "An introduction to single-point closure methodology, introduction to the modeling of turbulence", *Lecture Series 1987-06*, Von Karman Institute for Fluid Dynamics.

Leonard, B.P. (1979), "A stable and accurate convective modelling procedure based on quadratic upstream interpolation", *Comp. Meth. Appl. Mech. Eng.*, Vol. 19, pp. 59-98.

Özisik, M.N. (1977), *Basic Heat Transfer*, McGraw-Hill, Tokyo.

Patankar, S.V. (1980), *Numerical Heat Transfer*, McGraw-Hill.

Patankar, S.V., Liu, C.H. and Sparrow, E.M. (1977), "Fully developed flow and heat transfer in ducts having streamwise-periodic variations of cross-sectional area", *J. Heat Transfer*, Vol. 99, pp. 180-6.

Prata, A.T. and Sparrow, E.M. (1984), "Heat transfer and fluid flow characteristics for an annulus of periodically varying cross-section", *Num. Heat Transfer*, Vol. 7, pp. 285-304.

Raithby, G.B. and Schneider, G.E. (1988), "Elliptic systems: finite difference method II", in Minkowycz, W.J., Sparrow, E. M., Schneider, G.B. and Pletcher, R.H. (Eds), *Handbook of Numerical Heat Transfer*, Chapter 7.

Rokni, M. and Sundén, B. (1996), "A numerical investigation of turbulent forced convection in ducts with rectangular and trapezoidal cross-section area by using different turbulence models", *Numerical Heat Transfer,* Vol. 30 No. 4, pp. 321-46.

Speziale, C.G. (1987a), "On non-linear K-l and K-ε models of turbulence", *J. Fluid Mechanics*, No. 178, pp. 459-75.

Stone, H.L. (1968), "Iterative solution of implicit approximations of multidimensional partial equations", *SIAM J. Number. Anal.*, Vol 5, pp. 530-58.

van Leer, B. (1974), "Towards the ultimate conservative difference scheme. II. Monotonicity and conservation combined in a second order scheme", *J. Comp. Phys.*, Vol. 14, pp 361-70.

Webb, B.W. and Ramadhyani, S. (1985), "Conjugate heat transfer in a channel with staggered ribs", *Int. J. Heat Mass Transfer*, Vol. 28 No. 9, pp. 1679-87.

Wilcox, D.C. (1993), *Turbulence Modeling for CFD*, DCW Industries, Inc.